

# Volume Catheter Parallel Conductance Varies Between End-Systole and End-Diastole

Chia-Ling Wei\*, *Member, IEEE*, Jonathan W. Valvano, *Member, IEEE*, Marc D. Feldman, Matthias Nahrendorf, Ronald Peshock, and John A. Pearce, *Senior Member, IEEE*

**Abstract**—In order for the conductance catheter system to accurately measure instantaneous cardiac blood volume, it is necessary to determine and remove the contribution from parallel myocardial tissue. In previous studies, the myocardium has been treated as either purely resistive or purely capacitive when developing methods to estimate the myocardial contribution. We propose that both the capacitive and the resistive properties of the myocardium are substantial, and neither should be ignored. Hence, the measured result should be labeled admittance rather than conductance. We have measured the admittance (magnitude and phase angle) of the left ventricle in the mouse, and have shown that it is measurable and increases with frequency. Further, this more accurate technique suggests that the myocardial contribution to measured admittance varies between end-systole and end-diastole, contrary to previous literature. We have tested these hypotheses both with numerical finite-element models for a mouse left ventricle constructed from magnetic resonance imaging images, and with *in vivo* admittance measurements in the murine left ventricle. Finally, we propose a new method to determine the instantaneous myocardial contribution to the measured left ventricular admittance that does not require saline injection or other intervention to calibrate.

**Index Terms**—Admittance, conductance catheter, finite-element model, parallel conductance, parallel myocardial admittance, phase angle measurement, ventricular volume.

## I. INTRODUCTION

**P**RESSURE-VOLUME analysis is an established method for assessing myocardial function. The left ventricular (LV) and right ventricular (RV) pressure-volume relationships are generated on a beat-by-beat basis during transient occlusion of the inferior vena cava to allow precise hemodynamic characterization of LV and RV systolic and diastolic function independent of loading conditions [1]–[3]. There is interest in applying ventricular pressure-volume relationships

to characterize gene-altered mice [6]. Conductance catheter measurement is one of the methods that can provide real-time pressure-volume analysis. However, the measurement of instantaneous volume has been problematic due to the small size of the mouse heart and its rapid rate (up to 700 bpm). Conductance technology has previously been miniaturized to generate an instantaneous conductance signal, which is proportional to volume, to solve this problem [4]–[8].

The conductance catheter system consists of a four-electrode (tetrapolar) catheter inserted into the mouse LV to generate an intraventricular electric field to continuously measure the instantaneous conductance change as the LV fills and ejects blood. Unfortunately, the measured conductance is a combination of LV blood and myocardium, but only the blood conductance should be used to estimate LV volume. Hence, the instantaneous parallel myocardial contribution must be determined and removed from the combined conductance signal.

Several methods have been developed to estimate the myocardial contribution to the total measured conductance, including saline injection and occlusion of the *vena cava*. All of these methods treat the myocardium as either purely resistive [1], [7], [9] or purely capacitive [10], even though the myocardium has been demonstrated to have both resistive and capacitive properties in the range of frequencies typically used for measurement, 1–100 kHz [11]–[15]. Furthermore, the myocardial resistive component is substantial [11]. Hence, the controversy has been whether or not the capacitive component is negligible compared to the resistive component in the frequency range of interest. We propose that both are significant, which makes it more appropriate to label the measured result the LV admittance, instead of LV conductance. In this paper, this hypothesis will be examined by measuring the magnitude and phase angle of the LV admittance. If the myocardial capacitance is negligible, the measured phase should be approximately 0°. If not, the phase angle should be measurable and should increase with frequency.

Further, it is reasonable to suspect that the fraction of total current reaching the myocardium varies between end-systole and end-diastole because the myocardium changes distance from the source electrodes [16]. Therefore, the myocardial contribution to the total measured admittance should change instantaneously throughout the cardiac cycle. However, previous literature does not include this effect in a satisfying way. The conductance catheter technique has long been said to have constant parallel conductance or current leakage into the myocardial wall throughout the cardiac cycle [9]. Hence, previous studies only determine a single steady state value for the parallel myocardial contribution to conductance [1], [4],

Manuscript received February 22, 2006; revised November 12, 2006.

\*C.-L. Wei is with the Department of Electrical Engineering, National Cheng Kung University, No. 1 University Road, Tainan 70101, Taiwan (e-mail: clwei@ee.ncku.edu.tw).

J. W. Valvano and J. A. Pearce are with the Department of Electrical and Computer Engineering, The University of Texas at Austin, Austin, TX 78712 USA (e-mail: valvano@mail.utexas; jpearce@mail.utexas.edu).

M. D. Feldman is with the Department of Medicine, The University of Texas Health Science Center at San Antonio, TX 78229-3900USA (e-mail: feldmanm@uthscsa.edu).

M. Nahrendorf is with the Cardiology Department, The University of Würzburg, Würzburg D-97074, Germany. He is now with Harvard Medical School, Boston, MA 02115 USA.

R. Peshock is with the Cardiology Department, The University of Texas Southwestern, Dallas, TX 75390 USA.

Digital Object Identifier 10.1109/TBME.2007.890732

[6], [7], [9]. Many investigators have used this finding; and it has, in part, been the basis for the acceptance of the technique to generate a reliable instantaneous LV volume signal even during changing loading conditions to generate end-systolic elastance. We question these assumptions and propose that the parallel myocardial admittance does change between end-diastole and end-systole, and is measurable.

We sought to address these issues by examining both the phase angle and magnitude of the measured LV admittance between end-systole and end-diastole at different frequencies. We performed both 3-D finite-element modeling studies and *in vivo* measurements in mice. Numerical models of the mouse LV were constructed from cardiac magnetic resonance imaging (MRI) images. A commercial finite-element software package, FEMLAB<sup>®</sup> (Comsol, Inc., Burlington, MA), was used to simulate and analyze the LV admittance signal. *In vivo* measurement of phase and magnitude of the total admittance between the two inner voltage-sensing electrodes of the tetrapolar catheter were also performed in mice. We demonstrate that the phase angle does increase with frequency and parallel myocardial admittance does change throughout the cardiac cycle. Our findings question the validity of arguments in the previous literature in favor of constant parallel conductance [9]. In addition, we also propose a method to determine the instantaneous parallel myocardial contribution to the total admittance signal.

## II. METHODOLOGY

### A. Three-Dimensional Mouse LV Model Constructed From MRI Images

Mouse thoracic MRI images were provided by the University of Würzburg in Germany and the University of Texas Southwestern Medical Center at Dallas. The mouse used to make the MRI images was a C57 black 6 at the age of 15 weeks. Each MRI slice is 1 mm thick. The field of view of those MRI images was  $3 \times 3$  cm with a matrix of  $256 \times 256$  pixels, each with an 8-bit grayscale. Most pixels have a grayscale value close to 0, or black, which makes it hard to see the profile of the LV, and especially hard to see the boundary of the myocardium. To enhance image contrast, we redistributed the pixel histogram to maximize the use of the 8-bit grayscale spectrum, from 0 to 255. The processed image is shown in Fig. 1(a) with both LV and RV indicated. The image shown in Fig. 1(a) was taken at end-diastole.

The blood/endocardial interface was extracted by thresholding at 140 in this case. However, the profile of the LV epicardial surface cannot be extracted by the same technique since its boundary is not as sharp. The Canny edge-detecting method was used to detect the epicardial surface [17]. This method prevents multiple responses/true edge, which is an advantage in edge localization. Fig. 1(b) shows the detected edges from Fig. 1(a). The shape of the LV myocardium is approximately a circle. The Hough transform [18] was used to determine the most appropriate circle to fit the edge pixels. The processed outlines of both LV blood and myocardium are shown in Fig. 1(c) for an example slice at approximately the major diameter of the LV.

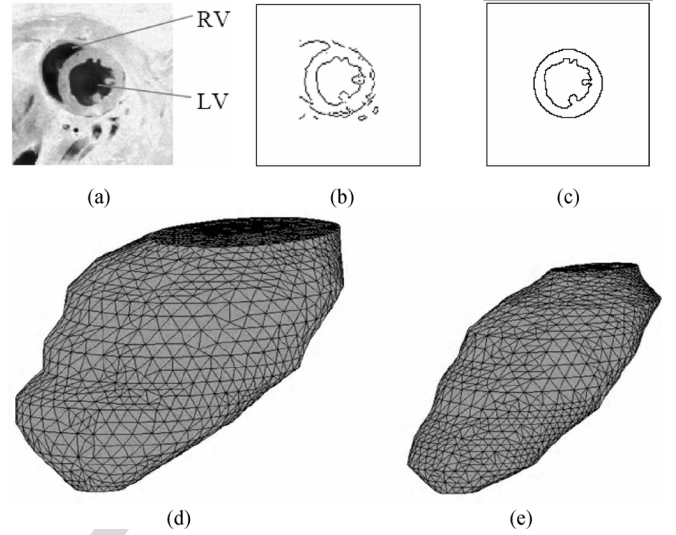


Fig. 1. (a) The enhanced MRI image at end-diastole (b) the detected edges by use of Canny method (c) the best-fit blood and myocardial outlines chosen by Hough transform, where RV is right ventricle and LV is left ventricle (d) mesh of myocardium in finite-element model (e) mesh of blood in finite-element model.

The 3-D LV finite-element model was constructed by stacking the blood and myocardial boundaries from the eight MRI images. The volume of the 3-D finite-element model can be calculated from

$$Vol = \sum_{i=1}^{n-1} \frac{(A_i + A_{i+1}) \cdot d}{2} \quad (1)$$

where  $n$  is the number of MRI images used for model construction,  $A_i$  is the endocardial area of the  $i$ -th MRI image, and  $d$  is the thickness of each MRI images. In our case,  $n$  is 8,  $d$  is 1 mm, the volume of the end-diastolic model is  $47.1 \mu\text{l}$ , and the volume of the end-systolic model is  $14.5 \mu\text{l}$ . By this method, the myocardial volume, i.e., the wall volume, can also be calculated. The wall volume is  $77.2 \mu\text{l}$  at end-diastole and  $76.1 \mu\text{l}$  at end-systole. There are three subdomains that impact the admittance measurement: myocardium, blood, and the conductance catheter. The finite-element meshes of the myocardium and blood are shown in Fig. 1(d) and (e). The catheter is modeled as 4 electrodes with interelectrode spacing of 0.5, 4.5, and 0.5 mm, respectively [Fig. 2(a)]. The passive components of the catheter are modeled as an insulating cylinder.

### B. Finite Element Models

The governing equation for this model is

$$\nabla \cdot [(\sigma + j2\pi f \epsilon) \nabla V] = 0 \quad (2)$$

where  $\sigma$  is the electrical conductivity (S/m),  $f$  is the frequency (Hz),  $\epsilon$  is the permittivity (F/m), and  $V$  is the scalar potential (V). This form is derived by combining Gauss electric law with the conservation of charge [16], [19]. The number of elements in the six finite-element models is between 32368 and 42820, and the respective degrees of freedom lies between 50416 and 66235. All simulations were properly converged. The finite-elements used in this model are quadratic. A linear iterative solver with drop tolerance of  $10^{-5}$  was used to make the calculation.

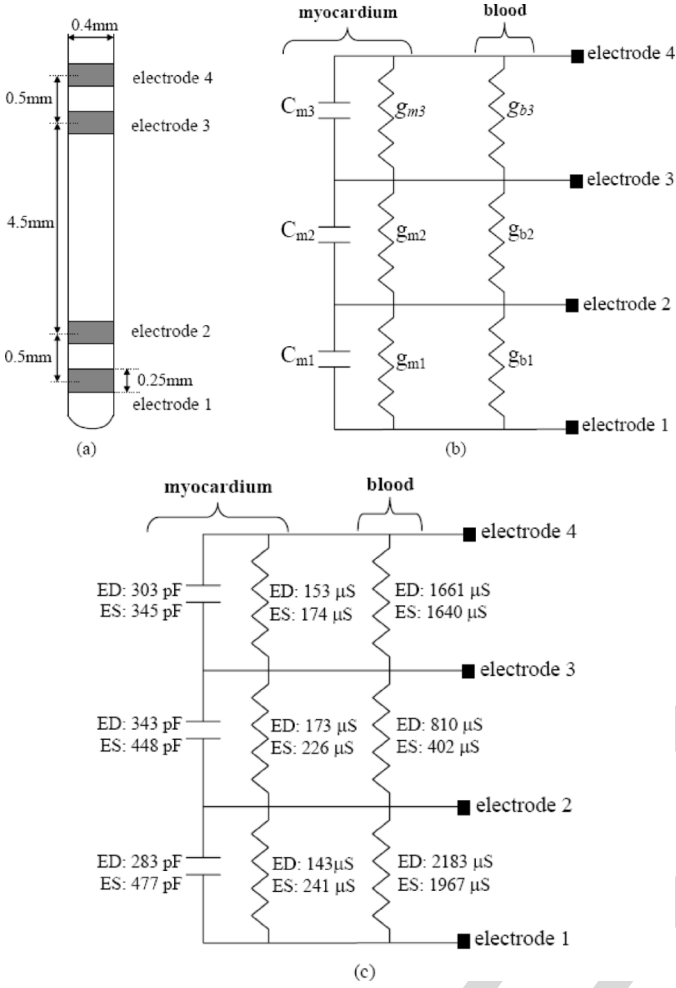


Fig. 2. (a) The illustration of the catheter physical size. The electrode spacing of the mouse conductance catheter used in simulation is shown. (b) the equivalent circuit model for mouse LV with component values derived from simulation. ED means the component value at end-diastole, ES stands for the value at end-systole,  $g_m$  is conductance of myocardium,  $g_b$  is conductance of blood, and  $C_m$  is capacitance of myocardium.

The model is submerged in an insulated space, so except for electrodes 1 and 4, the surface boundary conditions are

$$\vec{n} \cdot [(\sigma + j2\pi f\epsilon)\nabla V] = 0 \quad (3)$$

where  $\vec{n}$  is the normal vector to the surface boundary. Regarding electrodes 1 and 4

$$\text{Electrode 1 : } V = 0, \quad (4)$$

$$\text{Electrode 4 : } J = 238.7 \frac{\text{A}}{\text{m}^2} \quad (5)$$

where  $J$  is the current density ( $\text{A}/\text{m}^2$ ). This value of current density represents a total of  $30\text{-}\mu\text{A}$  (p-p) current through a 0.2-mm radius circle located on one end of the cylindrically shaped electrode, which is the current used to make these admittance measurements. In fact, the current density over the electrode surface is not uniform. It is denser around the edges of the electrode. To verify whether the uniform current density assumption in (5) is practicable, we also used a constant voltage source, which does not have this uniformity problem, to repeat the simulation. Both methods generated the same LV admittance

TABLE I  
ELECTRIC PROPERTIES IN EACH DOMAIN.

Domain	3D LV Model	
	Conductivity (S/m)	Permittivity (F/m)
Myocardium	0.17	$3.419 \times 10^{-7}$
Blood	0.93	$8.853 \times 10^{-9}$
Electrode	9661000	$8.854 \times 10^{-12}$

between electrodes 2 and 3. Hence, we can conclude that the assumption of uniform current density is justified for our studies.

The values of blood and myocardial conductivity and permittivity can be found in previous literature [14], [15]. Since these electrical parameters might change slightly from species to species, or even from strain to strain, an alternative method to determine those parameters is through dual frequency measurement. From our previous work, the apparent myocardial resistivity (the magnitude of the ‘‘impedivity’’) is  $5.754 \Omega\text{-m}$  at 10 kHz and  $3.630 \Omega\text{-m}$  at 100 kHz [20]. According to our hypothesis, the measured myocardial resistivity actually comes from myocardial conductivity  $\sigma_m$  and myocardial permittivity  $\epsilon_m$ . Their relationships at 10 and 100 kHz are

$$\frac{1}{5.754} = \sqrt{\sigma_m^2 + (2\pi \cdot 10^4 \cdot \epsilon_m)^2} \quad (6)$$

$$\frac{1}{3.630} = \sqrt{\sigma_m^2 + (2\pi \cdot 10^5 \cdot \epsilon_m)^2} \quad (7)$$

Then,  $\sigma_m$  and  $\epsilon_m$  can be estimated from (6) and (7) and are listed in Table I along with murine blood conductivity also obtained from our previous work [6]. The permittivity of blood is  $8.85 \times 10^{-9} \text{ F/m}$  [15]. Since both the blood and the electrodes are mainly conductive, the displacement current density in them is small and does not affect our simulation result significantly. Those parameters were used for both the finite-element model simulations and calculation of results from the *in vivo* experiments.

To reduce the computation time and memory required, both the blood and myocardial outlines are defined as either circles or ellipses as chosen from the Hough transform analysis of the slices. In other words, papillary muscles were ignored. To estimate the error due to ignoring the papillary muscles, we added an ellipsoid with approximately the same volume as the summation of papillary muscles to the myocardium for end-systolic and end-diastolic models. For the end-systolic model, the differences in magnitude and phase of the LV admittance between the electrodes pairs were 3% and 6%, respectively. For the end-diastolic model, the differences were less than 2% in both magnitude and phase. Therefore, ignoring papillary muscles does not significantly affect the total admittance between the electrodes pairs.

### C. Equivalent Circuit Models for the Mouse Left Ventricle

We propose an equivalent circuit model for the mouse LV, as is shown in Fig. 2(b). Blood is modeled by pure conductances,  $g_{bi}$ , and myocardium is modeled as conductances,  $g_{mi}$ , in parallel with capacitors,  $C_{mi}$ . Since the geometry of the LV is not symmetric, the values of those components in each segment are not likely to be the same.

In the FEMLAB<sup>®</sup> simulation, the electrode voltages are complex numbers due to the complex media. We denote the voltage at each electrode as  $V_1$ ,  $V_2$ ,  $V_3$ , and  $V_4$ , respectively. The current flowing through the electrodes is  $30 \mu\text{A}$  (p-p) as described above, with  $0^\circ$  phase angle. The myocardial capacitance can be calculated from the imaginary part of the total admittance between two adjacent electrodes, that is

$$C_{mi} = \frac{1}{2\pi f} \cdot \text{Im} \left\{ \frac{30\angle 0^\circ \mu\text{A}}{V_{i+1} - V_i} \right\}, \quad \text{for } i = 1, 2, 3. \quad (8)$$

In our experiments,  $f$  is either 10 or 100 kHz. From the electric field point of view,  $g_{mi}$  and  $C_{mi}$  are defined as

$$g_{mi} = \frac{I}{V} = \frac{\oint_A J \cdot dA}{-\int_L E \cdot dl} = \frac{\oint_A \sigma_m E \cdot dA}{-\int_L E \cdot dl} \quad (9)$$

$$C_{mi} = \frac{Q}{V} = \frac{\oint_A \varepsilon_m E \cdot dA}{-\int_L E \cdot dl} \quad (10)$$

where  $E$  is electric field,  $J$  is current density,  $I$  is current,  $Q$  is charge,  $A$  is the area of the surface enclosing the source electrode, and  $L$  is the path length for potential calculation. It is assumed that both  $\varepsilon_m$  and  $\sigma_m$  are approximately isotropic constants in the myocardium. While myocardial cells are actually highly anisotropic, the LV catheter averages its measurement over the thickness of the ventricular wall. The cells are oriented in many directions over the wall thickness, so the anisotropic effects are spatially averaged by the catheter measurement. Consequently, we suggest that the assumption of effectively isotropic parameters is reasonable and justified [20].

Combining (9) with (10) yields the well known conductance-capacitance analogy [19]

$$\frac{C_{mi}}{g_{mi}} = \frac{\varepsilon_m}{\sigma_m}. \quad (11)$$

Accordingly, the myocardial conductance can be calculated from its capacitance by

$$g_{mi} = C_{mi} \frac{\sigma_m}{\varepsilon_m}, \quad \text{for } i = 1, 2, 3. \quad (12)$$

The real part of the total admittance between the electrodes comes from blood and myocardial conductance; therefore:

$$g_{bi} = \text{Re} \left\{ \frac{30\angle 0^\circ \mu\text{A}}{V_{i+1} - V_i} \right\} - g_{mi}, \quad \text{for } i = 1, 2, 3. \quad (13)$$

$V_1$ – $V_4$  are all determined from simulation results, so the values of those components can be calculated from (8), (12), and (13).

However, only the magnitude and the phase of the total admittance between the two inner sensing electrodes will be measured in the *in vivo* experiments. As a result, only  $g_{m2}$ ,  $g_{b2}$ , and  $C_{m2}$  can be calculated in the experiments. We denote the total measured admittance as  $Y_{\text{meas}}$  and its phase as  $\phi$ , i.e.,  $Y_{\text{meas}} = |Y_{\text{meas}}| \angle \phi$ . Then,  $g_{m2}$ ,  $g_{b2}$ , and  $C_{m2}$  can be calculated from:

$$C_{m2} = \frac{|Y_{\text{meas}}| \cdot \sin(\phi)}{2\pi f} \quad (14)$$

$$g_{m2} = C_{m2} \frac{\sigma_m}{\varepsilon_m} \quad (15)$$

$$g_{b2} = |Y_{\text{meas}}| \cdot \cos(\phi) - g_{m2}. \quad (16)$$

The myocardium admittance  $Y_m$  then can be calculated by

$$Y_m = g_{m2} + j2\pi f C_{m2}. \quad (17)$$

In other words, the parallel myocardium contribution can be estimated by performing both phase and magnitude measurement at a single frequency. However, measurements at two frequencies are needed to calculate  $\sigma_m$  and  $\varepsilon_m$ , as shown in (6) and (7).

#### D. In Vivo Mouse Measurements

A 1.4-Fr pressure-volume catheter [SPR-839, Millar Instruments, Houston, TX, Fig. 2(a)] was used in these studies. The catheter has four 0.25-mm-length platinum electrodes with interelectrode spacing of 0.5, 4.5, and 0.5 mm, respectively. Since there is no instrument commercially available to measure both phase and magnitude signals for the murine conductance catheter measurement system, a custom-designed measurement system was built to do the task [22]. A combined 10- and 100-kHz sinusoidal signal generated from a separate function generator board was fed into an instrument designed by us (Fig. 3) and then converted into a current signal. A  $30\text{-}\mu\text{A}$  peak-to-peak excitation ac current, superposed 10 and 100 kHz, was applied to the two outermost electrodes to generate an intraventricular electric field. The voltage differences between the two inner electrodes were measured continuously. The magnitude of the voltage between the two inner electrodes is proportional to the impedance between the inner electrode pair. This dual-frequency signal was separated by two band-pass filters (BPF, Fig. 3) and amplified. These filtered signals together with the input signal were sampled by a digital oscilloscope (TDS 350, Tektronix). The oscilloscope communicates with the PC through a GPIB interface, as shown in Fig. 3. LabVIEW<sup>™</sup> 6.1 was used to record and MATLAB<sup>®</sup> was used to analyze the data. The phase measurement is not performed in real-time in this system. The oscilloscope was used to record 1000 samples at a sampling rate of 2 MHz for 10-kHz signals or 20 MHz for 100-kHz signals each time. In other words, the oscilloscope only can record 0.5 ms for 10-kHz signals or 0.05 ms for 100-kHz signals. Given a heart rate of a mouse is 700 bpm, there will be 85.7 ms/cardiac cycle. Thus, the duration of each record is less than 1% of the period of a cardiac cycle. Besides, the data recording process was triggered manually. The recorded data from both input and output signals were converted into the frequency domain by fast Fourier transform analysis. The measured phase is the phase difference between the input and output signals at either 10 or 100 kHz. The magnitude of the measured admittance is inversely proportional to the amplitude of the output signal. Moreover, in order to demonstrate the missing timing information of our system, a commercially available measurement system, MPVS-400, manufactured by Millar Instruments, was used simultaneously to record data. However, this system can only record pressure and magnitude signals, not phase signals.

Calibration is required for both magnitude and phase angle. Magnitude calibration was performed to convert the voltage output into conductance using known resistors to calibrate the instrumentation. Phase calibration was required to eliminate the phase shift due to the system electronics and to compensate

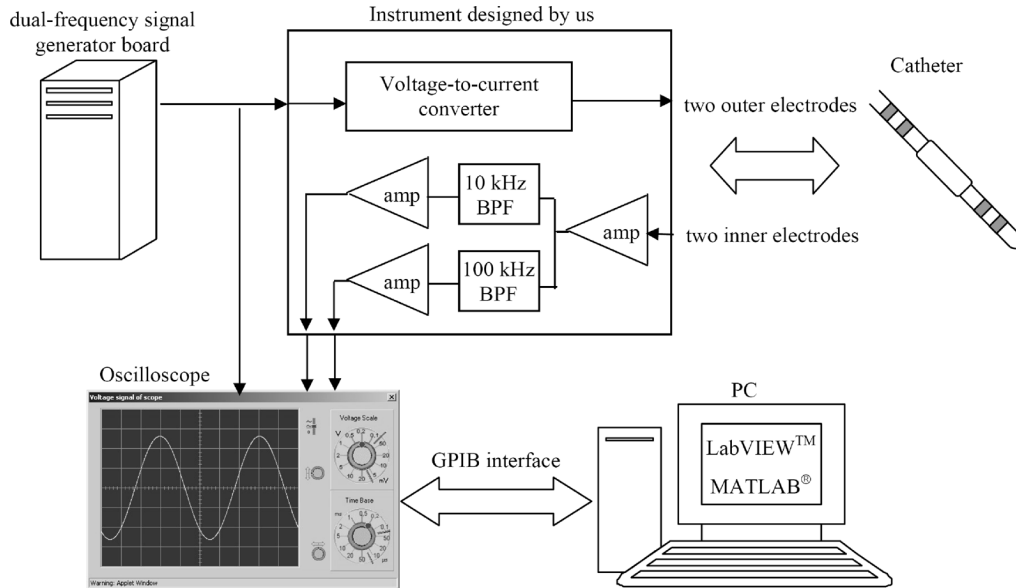


Fig. 3. The block diagram of dual-frequency phase measurement system.

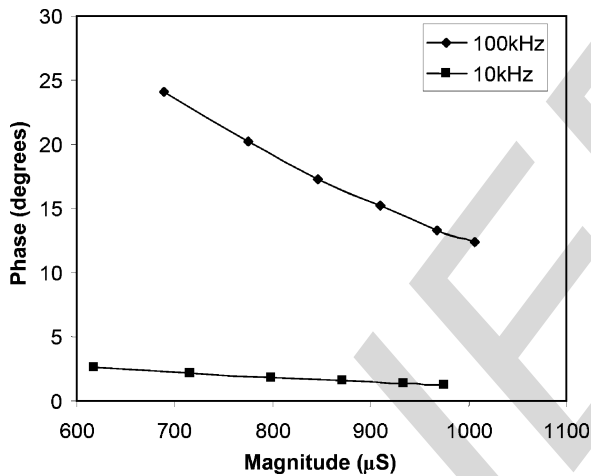


Fig. 4. Magnitude versus phase of the calculated LV admittance at 10 and 100 kHz.

the stray capacitance in the miniaturized mouse catheter, both of which were substantial. Phase calibration was performed by inserting the miniaturized mouse catheter into saline of known conductivities spanning the conductivity of murine blood and myocardium,  $816\text{--}10750 \mu\text{S}/\text{cm}$  [6].

The animal experiment protocol was approved by the Institutional Animal Care and Use Committee at the University of Texas Health Science Center at San Antonio. The protocol conformed with “Guidelines for the Care and Use of Laboratory Animals” (NIH publication No. 86–23, revised in 1985) and “Principles of Laboratory Animal Care” (published by the National Society for Medical Research). Six C57 black mice with weights of  $28.5 \pm 2.9\text{g}$  were anesthetized with urethane ( $1000 \text{ mg/kg IP}$ ) and etomidate ( $25 \text{ mg/kg IP}$ ). Respiration was controlled through a tracheotomy cannula, and the mice were mechanically ventilated with a rodent ventilator at 150

breaths/min supplemented with 100% oxygen. The chest was entered by anterior thoracotomy. A 30-gauge needle was used to make an apical stab in the heart, and then removed. The miniaturized mouse conductance catheter was advanced retrograde into the LV along the long axis with the proximal electrodes just within the myocardial wall of the apex.

#### E. Validation and Calibration of the Phase Measurement

Six cylindrical holes were drilled in a thick block of Plexiglas. The volumes of those holes span the typical volume range seen in a mouse LV ( $20\text{--}67 \mu\text{l}$ ), where the volume of a Plexiglas hole is defined as the solution volume between the two inner electrodes, 2 and 3 in Fig. 2(a). The conductivity of KCl solution used to fill those holes was  $1.50 \text{ S/m}$  at  $23^\circ\text{C}$  (room temperature). The catheter was inserted into the center of the solution-filled cylindrical hole and fixed. The block of plexiglas is placed on a platform whose height is adjustable to control the depth of catheter in the solution. This experiment was performed to prove that the instrumentation does not introduce different artificial phase shifts when measuring different volumes.

### III. RESULTS

#### A. Femlab® Simulation Results

Six finite-element models were assembled to represent the mouse LV at different times during the cardiac cycle. Table II summarizes the properties of the models for end-diastole and end-systole. Calculated admittance is the total admittance between the two inner sensing electrodes, 2 and 3. The equivalent circuit models at end-diastole and end-systole are illustrated in Fig. 2(c) and Table III. Fig. 4 shows the relationship between magnitude and phase of the calculated admittance determined from six models throughout the cardiac cycle. As the magnitude increases, the phase angle decreases at both 10 and 100 kHz. The phase angle calculated at 100 kHz is consistently larger than that at 10 kHz, as expected.

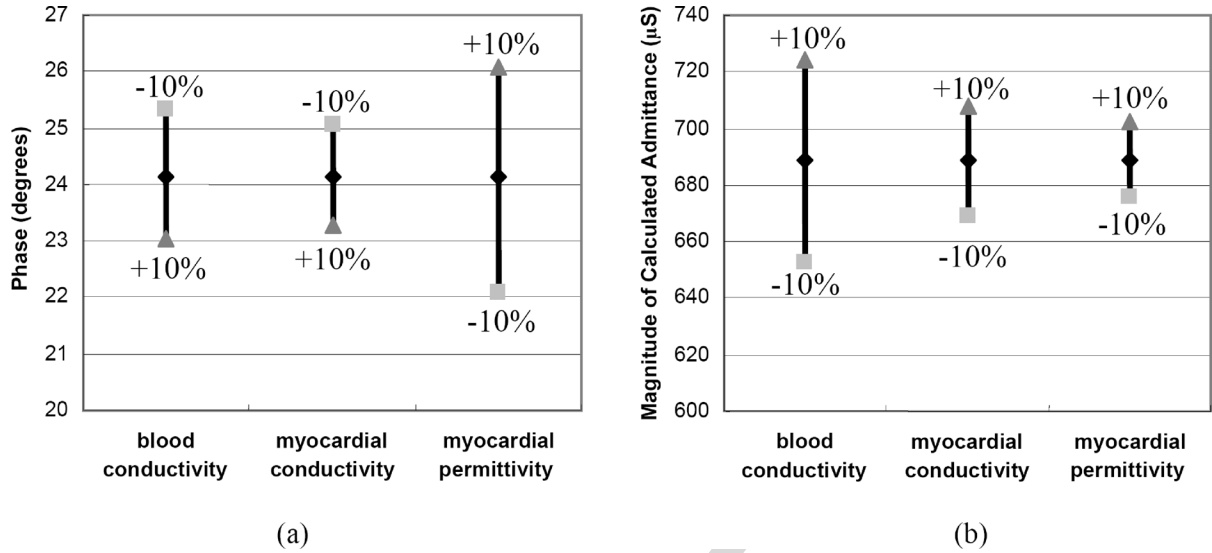


Fig. 5. Sensitivity analyses of the calculated LV admittance with respect to blood conductivity, myocardial conductivity, and myocardial permittivity for (a) phase (b) magnitude.

TABLE II  
END-DIASTOLIC AND END-SYSTOLIC FINITE ELEMENT MODELS.

	End-diastole	End-systole
LV volume ( $\mu\text{L}$ )	47.1	14.5
Magnitude of calculated admittance at 10kHz ( $\mu\text{S}$ )	976.0	617.2
Magnitude of calculated admittance at 100kHz ( $\mu\text{S}$ )	1006.8	688.5
Phase of calculated admittance at 10kHz	1.27°	2.64°
Phase of calculated admittance at 100kHz	12.36°	24.13°

### B. Sensitivity Analyses of the Femlab® Model

The end-systolic finite-element model simulation at 100 kHz was chosen for sensitivity analysis. Three parameters, blood conductivity, myocardial conductivity, and myocardial permittivity, were all decreased and increased by 10%. The corresponding changes in the phase angle and the magnitude of the calculated admittance are illustrated in Fig. 5. The phase is most sensitive to myocardial permittivity, while the magnitude is most sensitive to blood conductivity, as would reasonably be expected. In particular, the phase angle increases with decreasing blood and myocardial conductivity, but decreases with decreasing myocardial permittivity, as expected. When the myocardial permittivity increases by 10%, the phase increases by 8.1%. When the blood conductivity increases by 10%, the magnitude increases 5.2%.

### C. Phase Angle Calibration

Fig. 6 shows the phase measurements in saline of different conductivities, spanning those seen in mouse blood and myocardium. Each point shown in Fig. 6 is the average of five measurements. The standard deviations are all less than 1° for

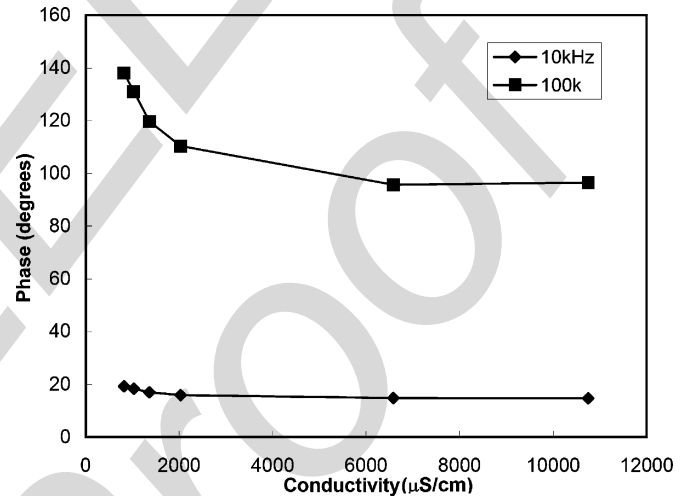


Fig. 6. Phase calibration measurements in saline of known conductivities. Mouse blood conductivity is approximately 10750  $\mu\text{S}/\text{cm}$ . Each point is the average of five measurements. The standard deviations are all less than 1° for measurements at 10 kHz and less than 3° for measurements at 100 kHz.

measurements at 10 kHz and less than 3° for measurements at 100 kHz, and are too small to be seen as error bars in the plot. The measured phase angle comes from the electronic circuit and catheter stray capacitance, since saline is purely resistive. The measured phase angle approaches a steady value for both 10 and 100 kHz, when the saline conductivity exceeds 4000  $\mu\text{S}/\text{cm}$ . The phase angle measured in saline at 10750  $\mu\text{S}/\text{cm}$ , which approximates murine blood conductivity, was used to compensate the *in vivo* phase measurements to eliminate the phase shift due to the instrumentation.

Fig. 7 is the phase angle measured in different-sized cylindrical holes filled with KCl solution ( $\sigma = 1.5 \text{ S}/\text{m}$ ). The phase angle does not change with solution volume at both 10 and 100 kHz, confirming that the instrumentation and catheter does not

TABLE III  
COMPONENTS IN EQUIVALENT CIRCUIT MODELS AT END-DIASTOLE AND END-SYSTOLE FROM FINITE-ELEMENT MODELS AND *IN VIVO* MICE MEASUREMENT DATA

	End-diastole				End-systole			
	Model	Mouse 1	Mouse 2	Mouse 3	Model	Mouse 1	Mouse 2	Mouse 3
Phase of admittance at 100kHz	12.4°	14.8°	15.4°	16.9°	24.1°	24.1°	20.5°	25.7°
Magnitude of admittance at 100kHz ( $\mu\text{S}$ )	1006.8	1061.5	942.2	1020.6	688.5	849.0	721.8	801.1
Myocardial conductance $g_{m2}$ ( $\mu\text{S}$ )	173	214	197	235	226	275	200	275
Myocardial capacitance $C_{m2}$ (pF)	343	431	397	473	448	552	401	552
Blood conductance $g_{b2}$ ( $\mu\text{S}$ )	810	812	711	741	402	500	477	447
Magnitude of myocardial admittance at 100 kHz $ g_{m2} + j2\pi f C_{m2} $ ( $\mu\text{S}$ )	276.5	345.6	318.2	378.7	361.0	442.4	321.7	442.5

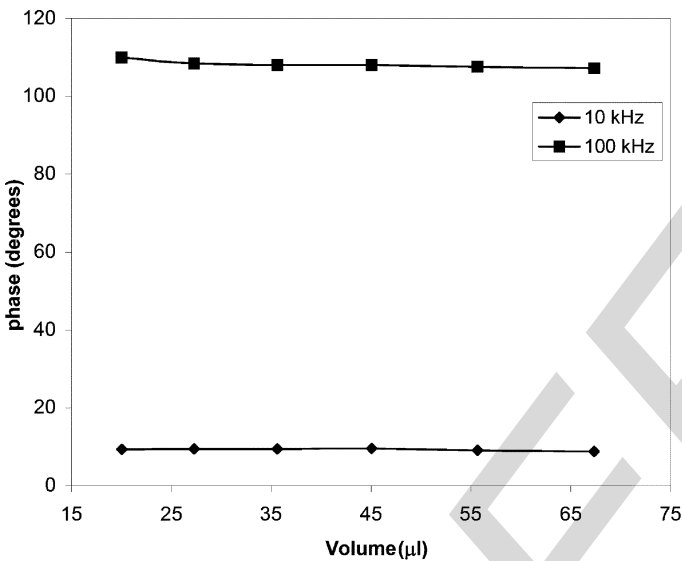


Fig. 7. The phase measured in different-sized holes filled with KCl solution.

introduce different phase angles when measuring different solution volumes.

#### D. *In Vivo* Mouse Phase Measurements

The phase angle measured at 10 kHz ranges from approximately 4° to 7° and the phase angle at 100 kHz ranges from 10° to 25°. The relationships between the phase and the magnitude of the measured LV admittance in three mice, and their corresponding LV pressure-magnitude loops are shown in Fig. 8. These mice were chosen because they have larger ranges in measured phase or magnitude, which means that their data are most likely to include true end-diastole and end-systole. In order to recover some timing information, magnitude-pressure plots recorded by MPVS-400 are also shown along with the magnitude-phase plots. With both types of plots, the corresponding phases of the cardiac cycle for the measured magnitude and phase signals can be retrieved. As a general trend, when the magnitude of the measured admittance increases, its phase angle tends to be smaller. From the simulation data shown in Fig. 4, the magnitude-phase relationship is not linear. Therefore, instead of linear lines, exponential curves provided a good fit to the data and were added to emphasize this trend (Fig. 8).

#### E. Equivalent Circuit Models From *in Vivo* Mouse Measurements

Table III compares the modeling and *in vivo* measurement results of three mice. The phase measured at 10 kHz is small (around 4°–7°), so that slight phase calibration inaccuracy affects the measurement significantly. Thus, data at 100 kHz were chosen for demonstration purposes. Two endpoints of the fitting curves were selected to represent end-diastole and end-systole, respectively. Using (14)–(16), the values of  $g_{b2}$ ,  $g_{m2}$ , and  $C_{m2}$  were calculated and are listed in Table III. The values from the FEMLAB® simulation are also listed for comparison and are similar. Agreement between the modeling and *in vivo* studies has been demonstrated.

## IV. DISCUSSION

Both the FEMLAB® simulation results and the *in vivo* mouse experiments show that the phase angle at 100 kHz is larger than the phase at 10 kHz (Figs. 4 and 8 and Table II), which demonstrates our hypothesis: the phase angle is measurable and increases with frequency. When frequency increases, the imaginary part of the total admittance, coming only from the myocardial capacitance, becomes larger, and the real part is unchanged. Therefore, the phase angle increases at higher frequency. These findings are consistent with the complex nature of the electrical properties of myocardium between 10 and 100 kHz [11], [14], [15].

In addition, the simulation results show that the magnitude of the calculated LV admittance increases with volume, which is consistent with the measured LV admittance being proportional to LV volume. However, the phase angle decreases with increasing volume (Figs. 4 and 8). At larger LV volumes, the distance between the myocardium and the source electrodes is greater, which makes the electric field weaker in the myocardium and decreases the fraction of measurement current flowing through the myocardium. Instead, a higher percentage of the current flows through the LV blood. As a result, the capacitive effects from the myocardium are less significant. On the other hand, the blood conductance, which dominates the real part of total admittance, increases with increasing volume. Therefore, the phase angle decreases with increasing LV volume.

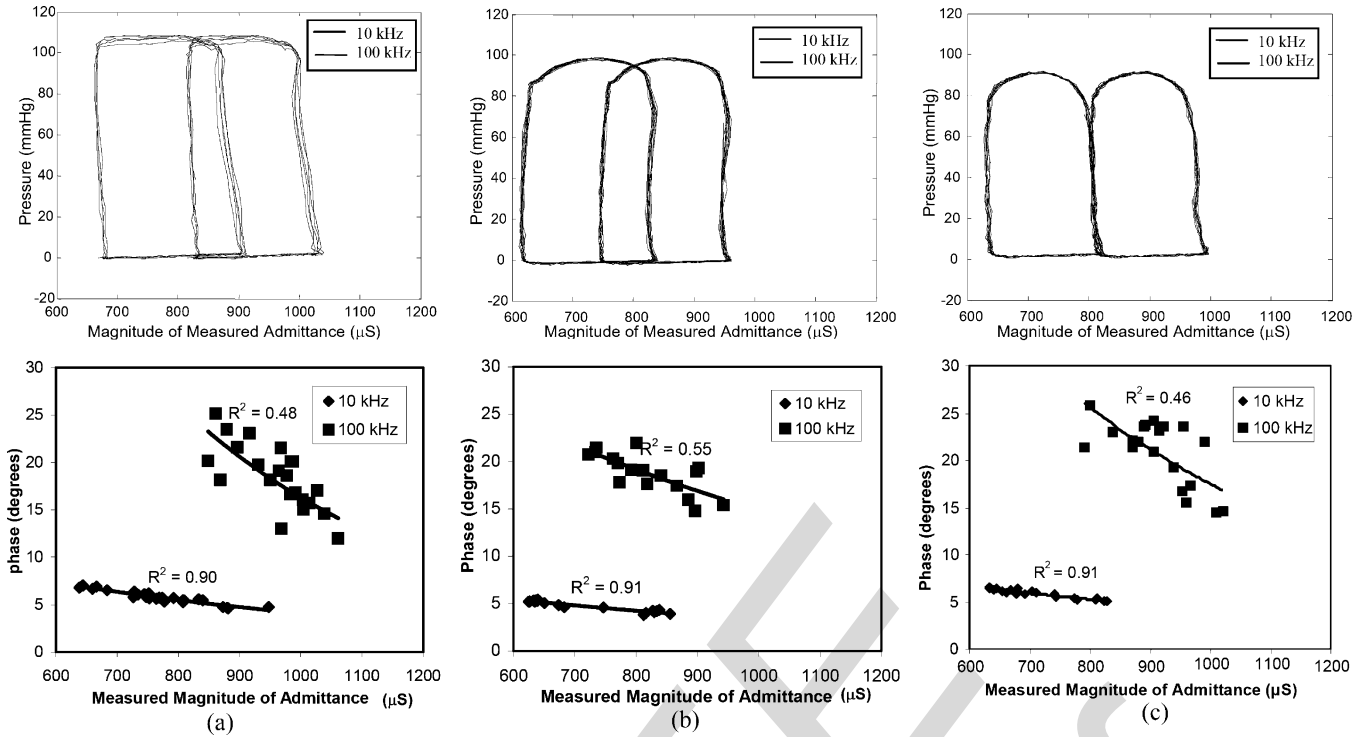


Fig. 8. The magnitude-pressure and magnitude-phase relationships of the LV admittance measured at both 10 and 100 kHz for three mice.

The KCl solution experiments were performed to demonstrate that the phase difference measured *in vivo* in a cardiac cycle does not come from the instrumentation. The volumes of the measured KCl solution are similar to those seen in a mouse LV, and both KCl solution and blood are purely resistive. The difference from the *in vivo* condition is that Plexiglas is non-conductive with very low permittivity, so no measurable current flows in it. The results show that the measured phase angle does not change with KCl solution volumes at the same frequency (Fig. 7), which proves that the instrumentation itself does not introduce an artificial phase shift when measuring different volumes.

Further insight regarding the interplay of blood conductivity, myocardial conductivity and myocardial permittivity was provided by sensitivity analyses (Fig. 5). Blood conductivity is the major factor determining the magnitude of calculated LV admittance, since blood conductance dominates the resulting admittance. On the other hand, myocardial permittivity plays a more important role in the phase angle of calculated LV admittance, because the phase signals originate from the myocardial capacitance alone, which is determined by myocardial permittivity. Changing either blood or myocardial conductivity will affect the real part of the calculated admittance, which in turn influences the phase angle. However, the effects are not as significant as myocardial permittivity. In fact, these three parameters may vary somewhat among individual mice, so the sensitivity analyses provide an explanation for the differences observed between numerical models and *in vivo* measured data (Table III).

According to previous literature [15], the myocardial conductivity and permittivity vary in the frequency range between 1 Hz and 1 GHz. Since the frequency range of our measurements (10 ~ 100 kHz) is relatively small, we assume that those param-

eters are unchanged in (6) and (7). However, this is a limitation of our study.

One disadvantage of this phase angle measurement instrumentation system is that we could not continuously measure the phase throughout the cardiac cycle. As stated above, the period of each recording phase is much less than 1% of the period of a cardiac cycle. Thus, we performed as many phase measurements as possible (20–30 measurements/frequency/mouse over many cardiac cycles) to cover as many of magnitude-phase points in the cardiac cycle as possible. However, the measurements may have missed true end-systole and end-diastole. Recognizing this limitation, we used the rationale that the larger the range of the measured phase or magnitude was, the more likely the measured data captured true end-diastole and end-systole. Using this rationale we chose the particular three mice out of the total of six for Fig. 8 and Table III. Fig. 8 demonstrates the success of this rationale.

The magnitude of the measured admittance is proportional to LV blood volume. Therefore, if the phase is plotted versus the magnitude of the measured admittance as shown in Fig. 8, the timing during the cardiac cycle of the measured phase is evident, i.e., the largest admittance occurs at end-diastole. As demonstrated from the FEMLAB<sup>®</sup> simulation shown in Fig. 4, the relationship between the magnitude and the phase of the LV admittance is not linear. Therefore, instead of linear regression lines, exponential curves were added in Fig. 8 to emphasize this trend. Further, the same timing shift caused by sampling jitter makes a phase error at 100 kHz ten times larger than that at 10 kHz. Therefore, the noise sensitivity at 100 kHz is at least ten times larger, which may explain the correlation coefficients at 100 kHz being lower than those at 10 kHz.

Table III compares the mouse LV equivalent circuit models derived from the FEMLAB<sup>®</sup> simulation results with the *in vivo* measurements. The values of blood conductance, myocardial conductance and myocardial capacitance from both methods are similar. The myocardial admittance at end-systole is not the same as that at end-diastole, which means that the parallel myocardial contribution is not constant during the cardiac cycle. In fact, the myocardial contribution to the total measured admittance is more significant at smaller LV volumes, as we would expect. Finally, if both phase angle and magnitude can be measured in real-time, instantaneous parallel myocardial admittance can be calculated by [(14)–(17)] and then removed from the total measured admittance. Actually, the myocardial admittance values shown in Table III are calculated by this new method. This would provide a new technique to determine the instantaneous myocardial contribution to the LV admittance signal without saline injection or other intervention. An improved impedance-based method with pressure measurement could be used to generate values of LV contractility, such as end-systolic elastance, effective arterial elastance, and diastolic compliance. Generation of these parameters in the pressure-volume plane requires transient occlusion of the inferior *vena cava* and a measure of the instantaneous increase in parallel myocardial admittance as the LV shrinks on a beat-by-beat basis.

It would be much more powerful if we could provide a validation of the actual measured volumes to demonstrate that the admittance measurement is superior to other methods, such as single frequency conductance. The currently accepted gold standard for *in vivo* murine left ventricular cardiac volume is MRI, which is not real-time though. However, a detailed comparison of single frequency conductance to admittance to determine that comes closest to the gold standard of MRI is a large and complex undertaking and well beyond the scope of the present study. However, we do concede the weakness of missing the volume validation studies in our work. Therefore, we included the finite-element models built from MRI images taken from the same strain of the experimental mice. In the numerical models, their volumes and admittances are known, unlike the experimental measurements. Because the experimental data and the simulation results agree closely, we can confirm that the ranges of the measured phase/magnitude and myocardial admittance *in vivo* are reasonable. By use of a proper conductance-to-volume equation, the LV volume can be accurately estimated [8].

## V. CONCLUSION

Three-dimensional numerical finite-element models for the mouse LV were constructed from mouse MRI images and then the magnitude and phase signals between electrodes were obtained by FEMLAB<sup>®</sup> simulations. In addition, *in vivo* phase and magnitude measurements were performed in mice. Both the results of the simulation and the *in vivo* experiments support our hypotheses: 1) both the capacitive and the resistive components of the myocardium are substantial and measurable in this frequency range; 2) the myocardial contribution to the total measured admittance is not constant throughout the cardiac cycle.

We proposed a method to derive the mouse LV equivalent circuit models from the simulation results and the *in vivo* experiments. We demonstrated that phase angle measurement together with magnitude measurement provides better insight into the electrical characteristics of mouse LV than the magnitude measurement alone. With the aid of phase angle and magnitude measurements, we also developed a method to determine the instantaneous parallel myocardial contribution to the total measured admittance. This paper provides the theoretical framework to allow phase angle measurements to be reduced to practice in the future to generate an instantaneous LV volume signal composed of blood alone.

## ACKNOWLEDGMENT

The authors would like to thank A. Kottam for his immense help with phase calibration experiments. They would also like to thank K. Raghavan, D. Altman, and D. J. Fernandez for their substantial contribution towards the instrumentation and the experimental measurements. They also thank M. Reyes, D. Escobedo and G. Freeman for their technical expertise concerning the animal experiments.

## REFERENCES

- [1] J. Baan *et al.*, "Continuous measurement of left ventricular volume in animals and humans by conductance catheter," *Circ.*, vol. 70, pp. 812–823, 1984.
- [2] K. Sagawa, L. Maughan, H. Suga, and K. Sunagawa, *Cardiac Contraction and the Pressure-Volume Relationship*. New York: Oxford Univ. Press, 1988.
- [3] D. Kass, M. Midei, W. Graves, J. Brinker, and W. L. Maughan, "Use of a conductance (volume) catheter and transient inferior vena caval occlusion for rapid determination of pressure-volume relationships in man," *Cath. Card. Diag.*, vol. 15, pp. 192–202, 1988.
- [4] D. Georgakopoulos, W. A. Mitzner, C. H. Chen, B. J. Byrne, H. D. Millar, J. M. Hare, and D. A. Kass, "In vivo murine left ventricular pressure-volume relations by miniaturized conductance micromanometry," *Am. J. Physiol. Heart Circ. Physiol.*, vol. 274, pp. H1416–H1422, 1998.
- [5] M. D. Feldman, J. M. Erikson, Y. Mao, C. E. Korcarz, R. M. Lang, and G. L. Freeman, "Validation of a mouse conductance system to determine LV volume: Comparison to echocardiography and crystals," *Am. J. Physiol. Heart Circ. Physiol.*, vol. 279, pp. H1698–H1707, 2000.
- [6] M. D. Feldman, Y. Mao, J. W. Valvano, J. A. Pearce, and G. L. Freeman, "Development of a multifrequency conductance catheter-based system to determine LV function in mice," *Am. J. Physiol. Heart Circ. Physiol.*, vol. 279, pp. H1411–H1420, 2000.
- [7] D. Georgakopoulos and D. A. Kass, "Estimation of parallel conductance by dual-frequency conductance catheter in mice," *Am. J. Physiol. Heart Circ. Physiol.*, vol. 279, pp. H443–H450, 2000.
- [8] C. L. Wei, J. W. Valvano, M. D. Feldman, and J. A. Pearce, "Nonlinear conductance-volume relationship for murine conductance catheter measurement system," *IEEE Trans. Biomed. Eng.*, vol. 52, no. 10, pp. 1654–1661, Oct. 2005.
- [9] E. B. Lankford, D. A. Kass, W. L. Maughan, and A. A. Shoukas, "Does volume catheter parallel conductance vary during a cardiac cycle?," *Am. J. Physiol. Heart Circ. Physiol.*, vol. 258, pp. H1933–H1942, 1990.
- [10] T. S. Gawne, K. S. Gray, and R. E. Goldstein, "Estimating left ventricular offset volume using dual frequency conductance catheters," *J. Appl. Physiol.*, vol. 63, no. 2, pp. 872–876, 1987.
- [11] P. A. White *et al.*, "The effect of changing excitation frequency on parallel conductance in different sized hearts," *Cardiovascular Research*, vol. 38, pp. 668–675, 1998.
- [12] H. P. Schwan, "Electrical properties of blood and its constituents: Alternating current spectroscopy," *Blut*, vol. 46, pp. 185–197, 1983.
- [13] J. Z. Tsai *et al.*, "In-Vivo measurement of swine myocardial resistivity," *IEEE Trans. Biomed. Eng.*, vol. 49, no. 5, pp. 472–483, May 2002.

- [14] C. Gabriel, S. Gabriel, and E. Corthout, "The dielectric properties of biological tissues: I. literature survey," *Phys. Med. Biol.*, vol. 41, pp. 2231–2250, 1996.
- [15] S. Gabriel, R. W. Lau, and C. Gabriel, "The dielectric properties of biological tissues: II. Measurements in the frequency range 10 Hz to 20 GHz," *Phys. Med. Biol.*, vol. 41, pp. 2251–2269, 1996.
- [16] C. L. Wei, J. W. Valvano, M. D. Feldman, M. Nahrendorf, and J. A. Pearce, "3D finite element complex domain numerical models of electric fields in blood and myocardium," in *Proc. IEEE Eng. Med. And Biol. Soc., 25th Annu. Int. Conf.*, Sep. 2003, pp. 62–65.
- [17] A. L. Bovik, *Handbook of Image & Video Processing*. San Diego, CA: Academic, 2000, pp. 426–428.
- [18] R. C. Gonzalez and R. E. Woods, *Digital Image Processing*. Reading, MA: Addison-Wesley, 1992, pp. 432–438.
- [19] D. K. Cheng, *Field and Wave Electromagnetics*. Reading, MA: Addison-Wesley, 1989, pp. 208–219.
- [20] M. Reyes *et al.*, "Impact of physiologic variables and genetic background on myocardial frequency-resistivity relations in the intact beating murine heart," *Am. J. Physiol. Heart Circ. Physiol.*, to be published.
- [21] J. G. Webster, *Medical Instrumentation: Application and Design*. New York: Wiley, 1999, pp. 183–230.
- [22] C. L. Wei, J. W. Valvano, M. D. Feldman, A. Kottam, D. Altman, K. Raghavan, D. J. Fernandez, M. Reyes, D. Escobedo, and J. A. Pearce, "Evidence of time-varying myocardial contribution by *in vivo* magnitude and phase measurement in mice," in *Proc. IEEE Eng. Med. Biol. Soc., 26th Annu. Int. Conf.*, Sep. 2004, vol. 2, pp. 3674–3677.
- [23] C. C. Wu, T. C. Skalak, T. R. Schwenk, C. M. Mahler, A. Anne, P. W. Finnerty, H. L. Haber, R. M. Weikle, and M. D. Feldman, "Accuracy of the conductance catheter for measurement of ventricular volumes seen clinically: Effects of electric field homogeneity and parallel conductance," *IEEE Trans. Biomed. Eng.*, vol. 44, no. 5, pp. 266–277, May 1997.
- [24] B. Gopakumaran, J. H. Petre, B. Sturm, R. D. White, and P. A. Murray, "Estimation of current leakage in left and right ventricular conductance volumetry using a dynamic finite element model," *IEEE Trans. Biomed. Eng.*, vol. 47, no. 11, pp. 1476–1486, Nov. 2000.
- [25] G. Mur and J. Baan, "Computation of the input impedances of a catheter for cardiac volumetry," *IEEE Trans. Biomed. Eng.*, vol. BME-31, no. 6, pp. 448–453, Jun. 1984.
- [26] P. Steendijk, E. T. van der Velde, and J. Baan, "Single and dual excitation of the conductance-volume catheter analyzed in a spherical mathematical model of the canine left ventricle," *Eur. Heart J.*, vol. 13, no. Suppl. E, pp. 28–34, 1992.



**Chia-Ling Wei** (S'01–M'04) received the B.S. and M.S. degrees both in electrical engineering from National Taiwan University, Taipei, Taiwan, in 1995 and 1997, and the Ph.D. degree in electrical and computer engineering from The University of Texas at Austin, in 2004.

She was with Silicon Laboratories Inc., Austin, TX, as a Design Engineer. She is currently an Assistant Professor at National Cheng Kung University, Tainan, Taiwan. Her researches are in the field of conductance catheter measurement system and

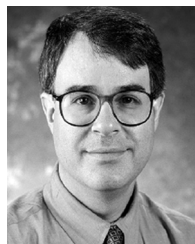
power management integrated circuit design.



**Jonathan W. Valvano** (M'83) was born in Clinton, CT, in 1953. He received the B.S. degree in computer science and engineering and the M.S. degree in electrical engineering and computer science from the Massachusetts Institute of Technology, Cambridge, in 1977. He received the Ph.D. degree in medical engineering from the Harvard University/MIT Division of Health Sciences and Technology in 1981.

He is currently a Full Professor at The University of Texas at Austin, performing research in the fields of perfusion measurements, bioinstrumentation, and

bioheat transfer models.



**Marc D. Feldman** received the B.S. degree from the Duke University, Durham, NC, in 1977, and the M.D. degree from the University of Pennsylvania School of Medicine, Philadelphia, in 1981.

He completed his internship and residency at Billings Hospital, University of Chicago, Chicago, IL, and did his fellowship training as a clinical and research fellow in cardiology at Beth Israel Hospital, Harvard Medical School, Boston, MA. He is currently Associate Professor of Medicine, Physiology and Engineering, Director of the Cardiac

Catheterization Laboratories, Division of Cardiology at The University of Texas Health Science Center at San Antonio. He is also an Adjunct Associate Professor at The University of Texas at Austin.



**Matthias Nahrendorf** was born in 1970 in Salzwedel, Germany. He received the <please specify full names and location(s) of institution(s) and degrees earned in what year(s) earned> from the Medical Schools of Heidelberg, London, and Bonn,

He took a position <please specify title?> at the Department of Internal Medicine, University of Wurzburg Hospital, Wurzburg, Germany, in 1999. Through 2004, he completed internship, residency, and fellowship, and was board licenced in internal medicine in 2006. In addition to his clinical career, he was also a Research Fellow with the Physics Department (EP5, Chair Axel Haase) focussing on small animal cardiac MR imaging. From 2004 to 2006, he was a Postdoctoral Research Fellow at the Center for Molecular Imaging Research, Massachusetts General Hospital, Harvard Medical School (CMIR, Chair R. Weissleder). In 2006, he took a faculty position at the CMIR, and is currently an Instructor in radiology and serves as the codirector of the mouse imaging program.



**Ronald M. Peshock** received the B.S. degree in mathematics from Michigan State University, East Lansing, in 1972 and the M.D. degree from the University of Texas Southwestern Medical Center, Dallas, in 1976.

He joined the faculty at the University of Texas Southwestern in 1982 and is now Professor of Internal Medicine and Radiology and Assistant Dean for Informatics. His research interests include magnetic resonance imaging in the evaluation of cardiovascular disease and early atherosclerosis and medical

informatics. He has authored and co-authored over 130 journal and invited papers.



**John A. Pearce** (M'78–SM'89) received the B.S.M.E. degree in 1968 and the M.S.M.E. degree in 1971 from Clemson University, Clemson, SC, and the M.S.E.E. degree in 1977 and the Ph.D. degree in electrical engineering in 1980 from Purdue University, West Lafayette, IN, .

He joined the faculty of Electrical and Computer Engineering at the University of Texas at Austin in 1982, where he is presently the Temple Foundation Professor (#3) in Electrical Engineering. His research interests include applications of electro-

magnetic fields in tissues and in industrial processes, impedance measurements in tissues, and tissue thermal damage studies.

Dr. Pearce is a member of the International Microwave Power Institute, the American Society of Mechanical Engineers, Eta Kappa Nu, Tau Beta Pi, and Phi Kappa Phi. He is also the editor in chief of the *Journal of Microwave Power and Electromagnetic Engineering*.